LA-11393-C, Suppl.
Conference

UC-414
Issued: January 1989

CONF-870 7124--Suppl.

LA--11393-C-Suppl.

DE89 006927

Supplement to the Neutron Resonance Radiography Workshop Proceedings

Los Alamos National Laboratory
July 27-29, 1987

Los Alamos National Laboratory
Los Alamos, New Mexico 87545

ABSTRACT

This publication is a supplement to *Neutron Resonance Radiography, Report of a Workshop Held at the Los Alamos National Laboratory July 27–29, 1987.*

Plasma Focus Sources

Vittorio Nardi and Jan Brzosko

Stevens Institute of Technology
Hoboken, NJ 07030

ABSTRACT*

Since their discovery, plasma focus discharges[1] have been recognized as very intense pulsed sources of deuterium-deuterium (D-D) or deuterium-tritium (D-T) fusion-reaction neutrons, with outstanding capabilities. Specifically, the total neutron emission/shot, Y_n, and the rate of neutron emission, $\dot{Y}_n$, of an optimized plasma focus (PF) are higher than the corresponding quantities observed in any other type of pinched discharge at the same level of powering energy W_0. Recent developments have led to the concept and experimental demonstration of an Advanced Plasma Focus System (APF)[2] that consists of a Mather-geometry plasma focus in which field distortion elements (FDEs) are inserted in the inter-electrode gap for increasing the neutron yield/shot, Y_n. The FDE-induced redistribution of the plasma current increases Y_n by a factor $\gtrsim 5$ - 10 above the value obtained without FDEs under otherwise identical conditions of operation of the plasma focus. For example, an APF that is fed by a fast capacitor bank with an energy, $W_0 = 6$ kJ, and voltage, $V_0 = 16.5$ kV provides $Y_n \cong 4 \times 10^9$ D-D neutrons/shot (pure D_2 filling) and $Y_n = 4 \times 10^{11}$ D-T neutrons/shot (filling is 50% deuterium and 50% tritium). The FDE-induced increase of Y_n for fixed values of (W_0, V_0), the observed scaling law $Y_n \propto W_0^2$ for optimized plasma focus systems, and our experience with neutron

---

* Work supported in part by AFOSR, Bolling AFB, D. C., and by ONR, Arlington, VA

scattering in bulk objects lead us to the conclusion that we can use an APF as a source of high-intensity neutron pulses (10^{14} n/pulse) in the field of neutron radiography (surface and bulk) with a nanosecond or millisecond time resolution. For instance, the estimated typical resolution in the case of a void in an iron plate 12-cm thick is 1 mm x 1 mm x 1 mm and 0.3 mm x 0.3 mm x 0.3 mm for a plate that is 1-cm thick.

An APF with $W_0 \cong 100$ to 200 kJ seems an ideal system for closing the gap between fission reactor sources and particle accelerator sources. Inductive field acceleration of ions and formation of high-density, magnetized plasma targets within extremely localized plasma regions in the APF pinch provide a point-like source where the bulk of the neutron-generating reactions are concentrated. This also gives the possibility of achieving high-resolution radiography without a collimator (and moderator) if a fast 14-MeV neutron-imaging system is available.

I. *Introduction*

Successful demonstrations of plasma focus machines as extremely intense pulsed sources of x-rays and neutrons from D-D fusion reactions were completed by the end of 1971. These demonstrations were done under both weapons-simulation and controlled nuclear-fusion programs for a wide range of values of the capacitor-bank energy W_0 ($W_0 \cong 1$ kJ - 0.4 MJ), which is normally used for feeding a focused discharge. A corresponding range of values of the neutron yield/shot, $Y_n \sim 10^8$ - 10^{12}, was obtained after optimization of the machine parameters (radius and length of the cylindric electrodes; inductance, L_t, of the powering system and electrode circuit; pressure P of the filling gas in the discharge chamber) for a fixed value of the capacitor bank voltage, V_0, and energy, W_0. More than forty laboratories worldwide have operated two versions of plasma focus machines—the J. Mather type and the N. V. Filippov type. Because the Fillippov type has an electrode system less compact than that of the Mather type and has slightly lower values of Y_n with wider fluctuation from shot-to-shot for a chosen value of W_0, we confine our presentation to the performance and characteristics of the Mather geometry.

A detailed description of ordinary plasma-focus systems is presented in the literature[1]. We list here only a few of the basic elements of the system and its modes of operation to explain the following: what has been done recently to increase Y_n and the phenomena that control Y_n. In our APF, Y_n is increased by a factor ≥ 5 - 10 as compared to the neutron

yield of an ordinary plasma-focus machine with the same electrode-geometry parameters and operating with the same value of W_0, V_0, and filling pressure, P. The characteristic and novel component of an APF is the field distortion element (FDE)[2]. An APF can be obtained by inserting an FDE in the interelectrode gap of an ordinary plasma focus machine. The FDE improves the quality of the current sheath; specifically, it sharpens the distribution of the interelectrode/plasma current by increasing the current-density peak in a thin current sheath of $\gtrsim$ 1-cm width in the axial direction. The evolution of the current sheath at all successive stages of the discharge critically depends on the initial conditions, which are established at the breakdown stage and are positively affected by a suitable FDE.

Conventional plasma-focus machines have been proposed also as neutron sources in radiation test facilities (10^{18} n/s, $W_0 > 5$ MJ) for the controlled thermonuclear reactor (CTR) surface and materials program[3]. Repetitive modes of operation have been considered (1 to 10 Hz and 10^5 Hz) in this context. Recent experiments[4] indicate that these repetitive modes can be used without great difficulties for relatively small PF machines, $W_0 \cong 1$ to 10 kJ. For neutron-radiography applications, an APF with $W_0 \cong 1$ to 200 kJ can provide a source with a high degree of mobility (as it is defined by the weight of the power supply and by the neutron moderator-collimator systems if slow-neutron radiography, instead of fast neutron radiography, is required). A maximum time resolution is achieved for fast neutrons, i.e., by using the APF without the moderator. In this case, the time resolution is of the same order of magnitude as the time width (FWHM) of the neutron pulse (about 50 ns). Neutron intensity and the small linear dimensions of the neutron source in an APF provide substantial advantages as compared to other accelerator-type, mobile sources. We limit our presentation to the basic features of an APF source—one that can be easily matched with a neutron moderator-collimator system and to the definition of imaging-resolution criteria, which are of some help for assessing the relative performance of different neutron sources in radiographic applications.

II. Plasma Focus Characteristics

A plasma focus system is usually formed by a pair of coaxial cylindric electrodes with an interelectrode gap of width $R_{0E} - R_{IE} \gtrsim 3 - 6$ cm, where a 1 - 2 μs discharge of peak current, $I_M \sim 10^5 - 10^6$ A, is established and fed by a high voltage, (V_0), low-inductance, (L_0), capacitor bank of energy

$$W = \frac{1}{2} C V_0^2 \quad ,$$

and peak electrode current,

$$I_M \cong \frac{V_0}{\sqrt{\frac{L_t}{C}}} \quad ,$$

where $L_t = L_0 + L_c$; L_c is the load inductance of the power-transmission-line interelectrode gap and plasma current sheath. At the onset of the discharge at the breech end of the electrodes, a current sheath is formed along the insulation sleeve surface, i.e., along the path of minimum inductance, and starts to propagate toward the muzzle end of the electrodes. Current sheath lift-off from the insulator surface and acceleration of the current sheath in the interelectrode gap is controlled by the force per unit surface of the current sheath $\underline{J} \times \underline{B}$. $\underline{J}$ is the current density on the current sheath and $\underline{B}$ is the magnetic field in the interelectrode gap behind the current sheath, which is generated by the electrode current.

A schematic of the electrode configuration of an APF (axial cross section) is shown in Fig. 1. The photograph of the coaxial electrode system and of the internal wall of the discharge chamber with two observation ports is shown in Fig. 2. The typical neutron yield/shot Y_n as a function of the peak electrode current [I_M, Fig. 3 (a)] and of the capacitor bank energy W_0 [Fig. 3 (b)] are reported in Fig. 3 from the experiments of leading laboratories. These data confirm a well-established scaling law[3] in terms of I_M and W_0:

$$Y_n \propto I_M^{\,m} \; (m = 4 \pm 0.4); \; Y_n \propto W_0^{\,n} \; (n = 2 \pm 0.2) \quad .$$

Image-converter photographs of the current sheaths (5-ns exposure times by visible light) during three final stages of the discharge are presented in Fig. 4. In Fig. 4 (a), the current sheath, with a typical filamentary structure, rolls off the muzzle end of the coaxial electrodes and implodes toward the electrode axis with a radial velocity, $V_r \cong 10^7$ cm/s; the axial pinch (where the high-intensity core of the neutron source is embedded) is presented in (b) during the maximum compression stage ~100 ns after (a); (c) shows the off-axis part of the current sheath about 50 ns after (b), when the pinch is disassembled and the neutron pulse is nearly extinguished.

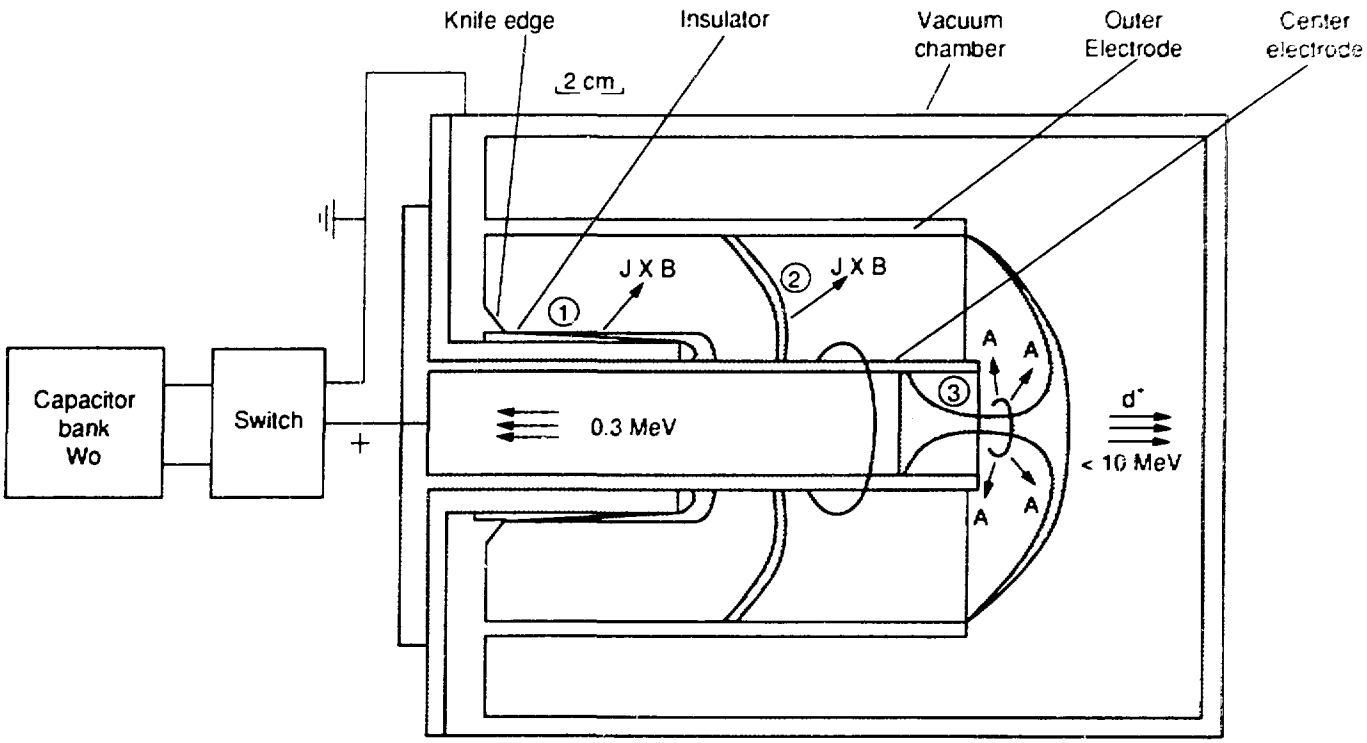

Fig. 1 Schematic view (axial cross section) of a Mather-type plasma focus machine with field distortion elements: APF (Advanced Plasma Focus) = PF with a field distortion element (here a circular knife edge of the breech).

The configuration of the current sheath, where the leading peak of the interelectrode current density is concentrated is outlined during the three main stages of the discharge:

1. Initial phase: gas breakdown, plasma-sheath formation and lift-off from the insulator.
2. Axial acceleration phase: the $\underline{J} \times \underline{B}$ force accelerates current sheath and accumulated mass.
3. Radial compression phase: typical pinch radius at maximum of radius compression $\equiv$ 2 mm.

Instabilities and high nuclear reactivity occur after phase 3 (Ref. 2).

Fig 2 (a) Discharge chamber (inside, front view) of an APF (max W_0 = 200 kJ) at Stevens Institute of Technology. The outer electrode is formed from 40 stainless steel bars. The wall of the vacuum chamber has a large diameter for diagnostic purposes, and the diameter of the hollow inner electrode (anode) is 11 cm

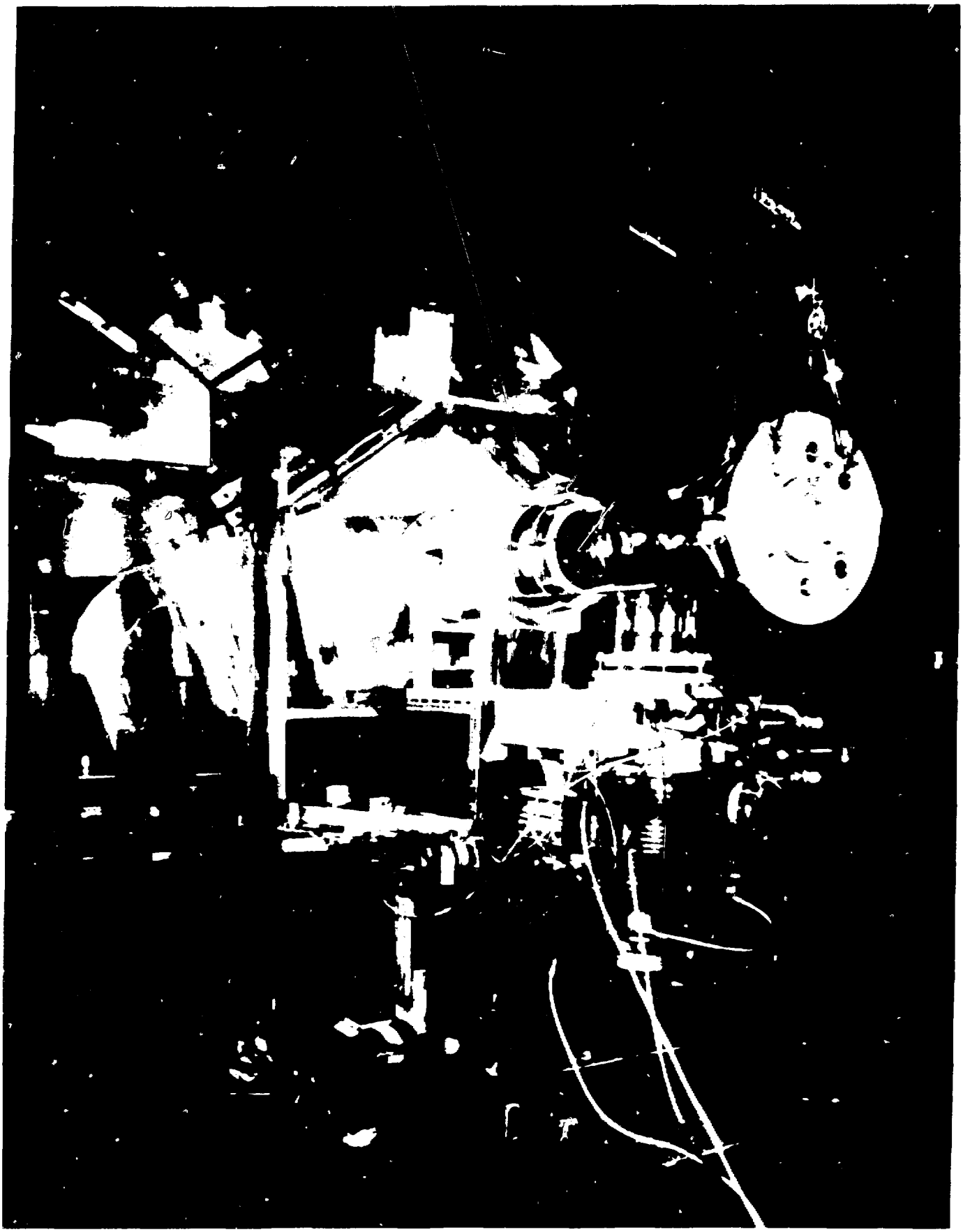

(b) View of the 200-kJ APF, presently under construction at Stevens Tech

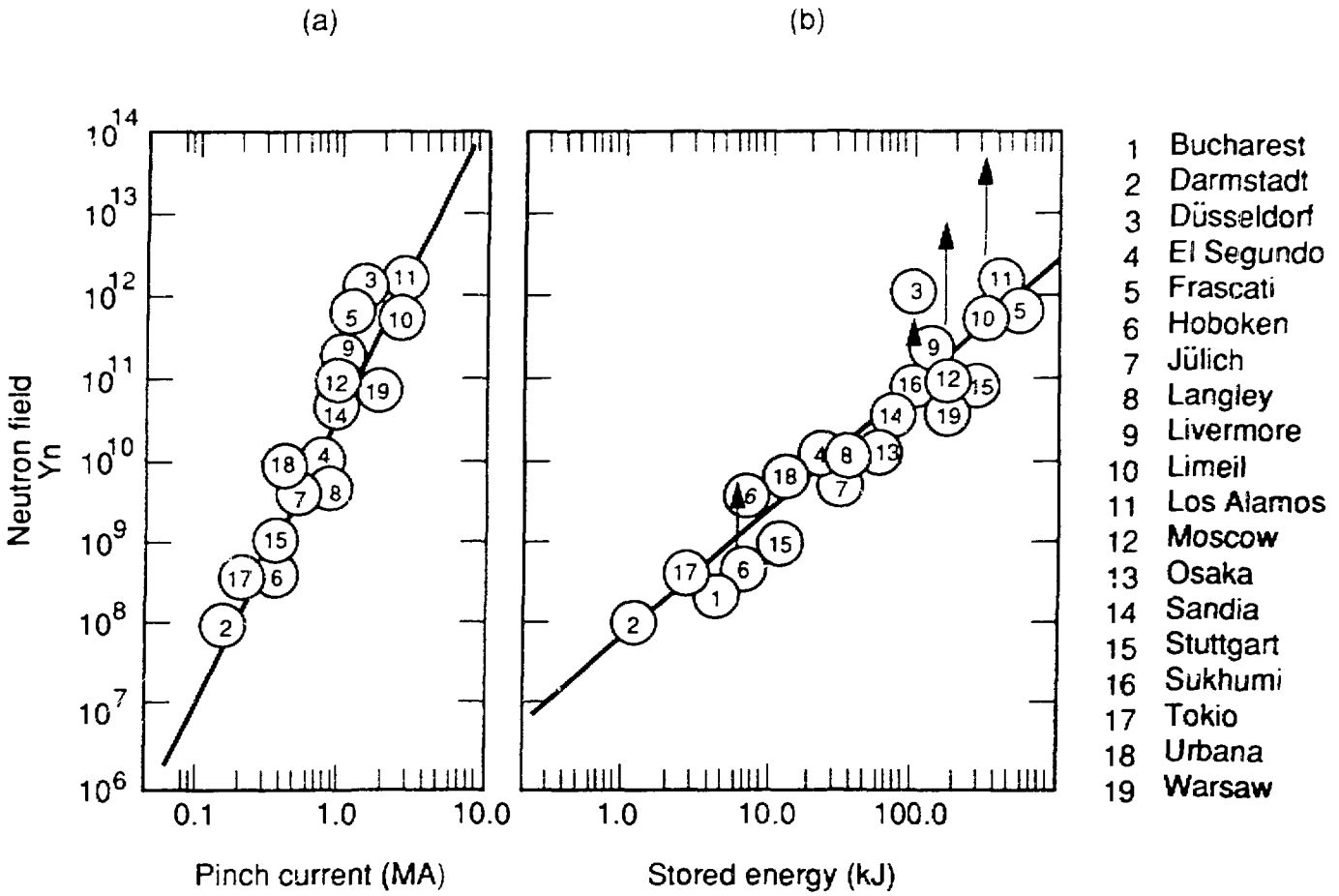

Fig. 3 Neutron yield Y_n (from D-D fusion reaction as a function of I_M, in (a), and of W_0, in (b)) *from different machines, which are operated in the laboratories listed on the left (log* scale). The vertical arrows (for 10, 16, 19) indicate the Y_n increase by a factor of ~100 observed by replacing the D_2 filling of the discharge chamber with a D_2-T_2 mixture. The arrow in 6 and the upper 6 indicate the Y_n increase by a factor 10 with field distortion elements at Stevens Institute of Technology. The scaling $Y_n \propto I_M^4$ ($Y \propto W_0^2$) holds with both D_2 and D_2-T_2 mixture fillings. The FDE-induced increase is expected to add up with the D_2-T_2 induced increase of Y_n.

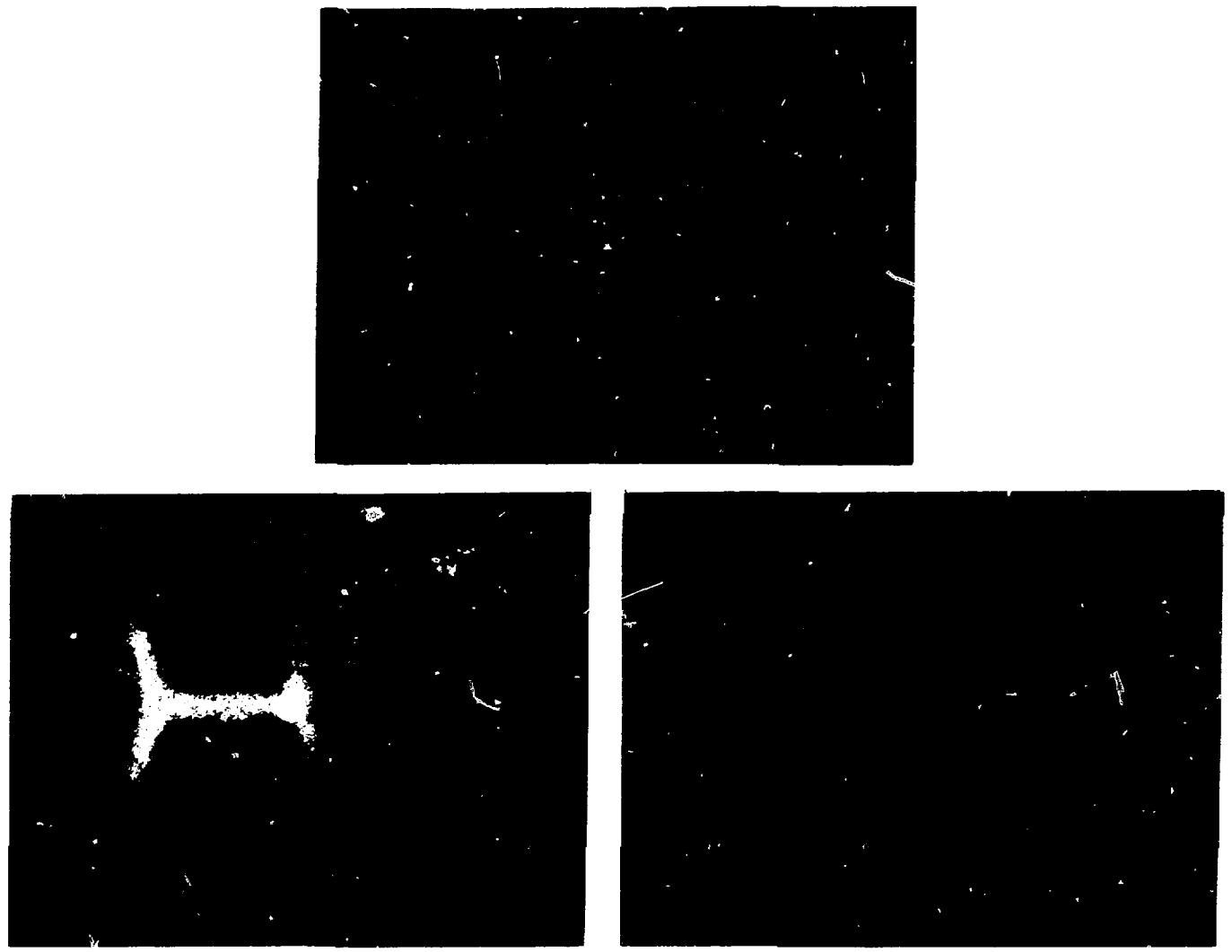

Fig. 4 Image-converter photograph by visible light (5-ns exposure time) of the current sheath of a 6-kJ PF at Stevens Tech. (a) Radial implosion stage (~200 ns before pinch formation); (b) Pinch formation (onset of neutron pulse); (c) 150 ns after pinch formation (the pinch is disassembled; the neutron pulse ends). The oscilloscope traces (100 ns/cm) indicate the time at which the current sheath photograph is taken. The sharp dip of the lower trace marks the exposure time with respect to the pinch-formation time, t_0, which is defined by the lowest point of dip in the upper trace from the electrode current signal. The oscilloscope traces correspond to the last two current-sheath photographs.

The main component of the neutron source is localized in one or two hot spots with linear dimensions ≤ 1 mm inside the axial pinch. A description of the space structure of the neutron source core, in which 80% of the total yield Y_n is generated[5], is given in terms of an x-ray pin-hole image[6,7,8] of the pinch (Fig. 5). Scintillation detector measurements with narrow-gap collimators (lead collimator for x-rays; 0.5-cm or 1-cm-gap paraffin collimator for neutrons) indicate that a neutron source and plasma x-ray source are coincident in space and time within experimental observations. The typical time structure of the neutron pulse with a full-width-at-half-maximum (FWHM) ≈ 20 ns is shown in Fig. 6 from the signal of an NE-102 detector inside a paraffin shield (the collimator gap is 1 cm wide and is orthogonal to the electrode axis) and, simultaneously, from an unshielded detector. The geometry of the collimator, detectors and source system is shown in Fig. 7.

The neutron emission is slightly higher at 0°, which is the forward direction of the electrode axis, than at 90°, with an anisotropy factor of 1.1 - 1.3, depending on the filling pressure, P, and V_0. The distribution of the number of shots as a function of Y_n is given in Fig. 8 for a $W_{0,H} = 6$ kJ (17 kV) APF (Hoboken in (a)[2]) and for a $W_{0,F} \geqq 250$ kJ (>20 kV) PF (Frascati, in (b)[9]) for P ≥ 3 Torr. The FDE in the APF reduces the FWHM of the event distribution by 30 - 40% as compared to a PF without an FDE. The narrowing of the distribution is observed by comparing (a) with the event distribution from the same machine in which the FDE has been removed (i.e., from a PF with the same W_0, V_0, P, etc.) The mean value, $Y_{n,H}$ from (a), is higher by a factor ~8 than the calculated value

$$Y_{n,H}^{C} = Y_{n,F} \cdot \left(\frac{W_{0,H}}{W_{0,F}}\right)^2$$

from the values $Y_{n,F}$, $W_{0,F}$ of (b). This is a clear advantage of using an APF over a PF.

By increasing the filling pressure to P = 6 Torr in the Y_n 6-kJ APF machine, Y_n increases to $Y_n = 1.1 \times 10^9$ for D-D fusion neutrons with a peak value, $Y_n = 4 \times 10^9$. By filling the discharge chamber with a mixture of 50% D_2 and 50% T_2 (by pressure), the neutron yield increases by a factor of 100 for all tested values of W_0 up to 200 kJ and is essentially composed of 14-MeV neutrons from D-T fusion reactions. Other methods for increasing the neutron yield, which can be combined with the increase from D-T mixtures, are

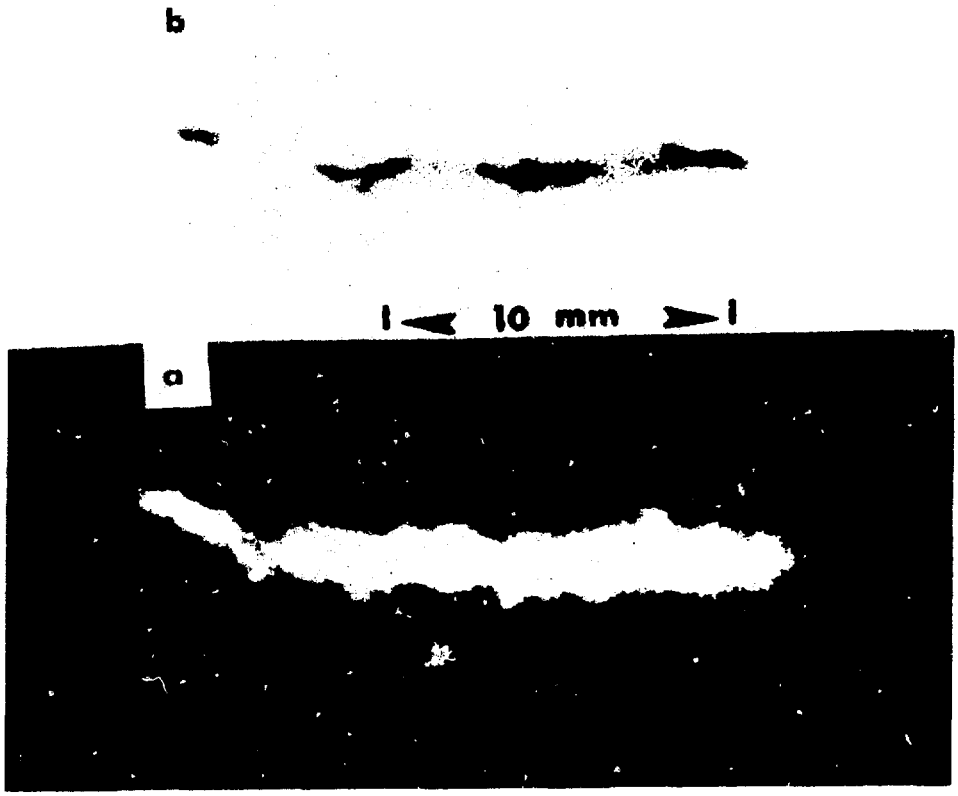

Fig. 5 (a) X-ray photography by pinhole (diam. 0.075 mm) camera at 50°; Be window, 0.018-mm thick, photon energy ≥ 1 keV; part of film is saturated. (b) X-ray radiography (magn.1:1) of film in (a). The internal structure of the x-ray source is resolved by this technique from saturated film[7]. Loops are visible at source borders in both images. This film-radiography method has been developed at the Univ. of Ferrara with the collaboration of the Material Science Division, Europ. Com. Commission Laboratory/Ispra (see P. Jehenson, F. Luchtmans: Proceed. 10th Nat. Conf. Nondestructive Tests, Salsomaggiore, Italy, 24-26 Oct. 1977).

The core of the x-ray source in (b)—with its strong peak of emission intensity—fits in space and time the neutron-source core, as determined from data obtained with paraffin and lead collimators (see Figs. 6 and 7). The typical cross section of the source core on the plane orthogonal to the electrode axis (0° view) has linear dimensions < 0.5 mm. Radiographic images in the axial direction (0° view) from the x-ray pulse of a PF machine without collimator have an excellent resolution[8]. A corresponding outstanding resolution is expected for radiographic images with fast (2.5 MeV or 14 MeV) neutrons if a suitable imaging system becomes available.

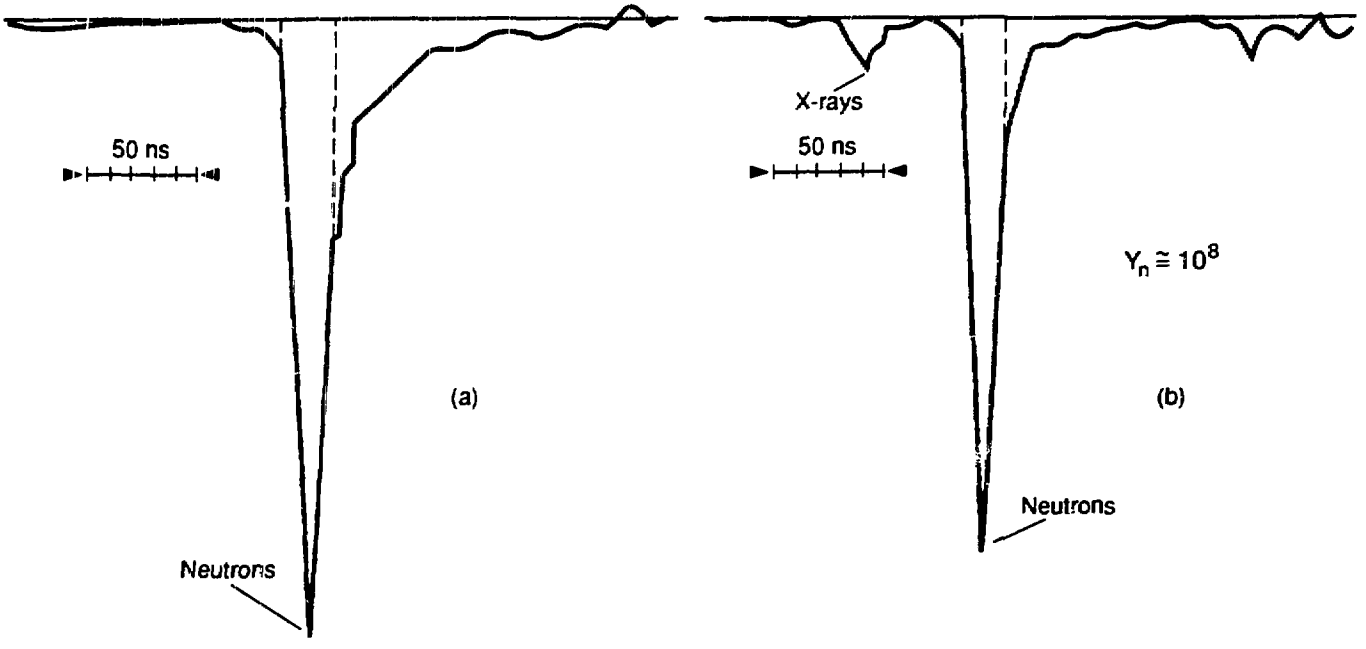

Fig. 6 Test on spatial extension of the neutron source along the electrode axis of a PF. Scintillation detector signal from (a) uncollimated and (b) collimated detectors (dashed lines separate peak area from tail area). Time increases from left to right (50 ns/cm); signal-amplitude scale is 0.2 V/cm in (a), 0.1 V/cm in (b); in the drawing the amplitude a_b of the signal in (b) is normalized to the same amplitude scale of (a). Neutron yield in this discharge is $Y_n \cong 10^8$ (conventional PF without FDE, D_2 filling, $W_0 = 5$ kJ; see Ref. 5 and Fig. 7).

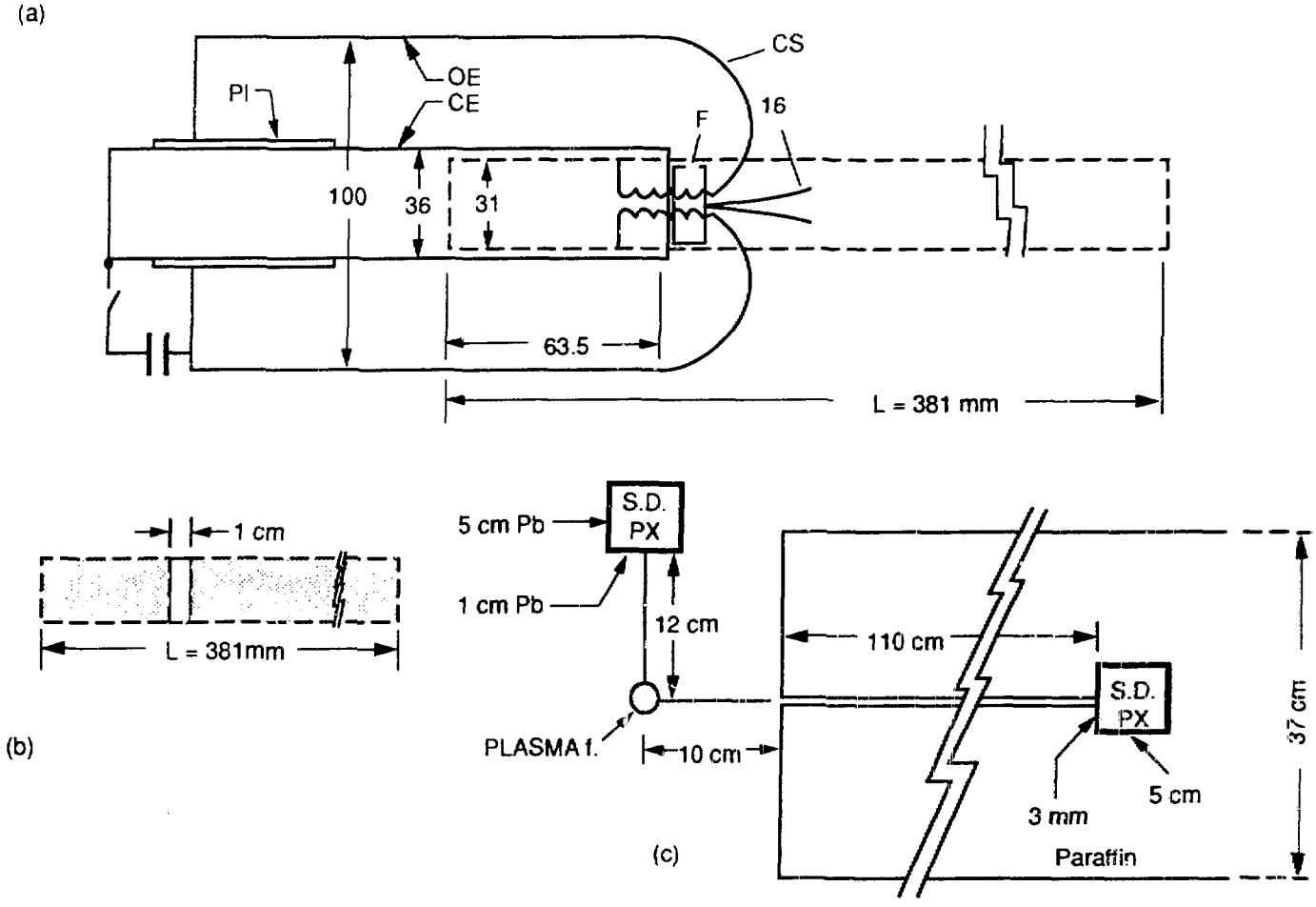

Fig. 7 (a) Schematic view of paraffin collimator, PF electrodes (DE, CE), off-axis part of current sheath (CS) and pinch location (F) where x-ray and neutron source are located. (b) Details of neutron collimator. (c) Arrangement of collimator and neutron detector (NE-102) with lead screen (see Fig. 6 and Ref. 5).

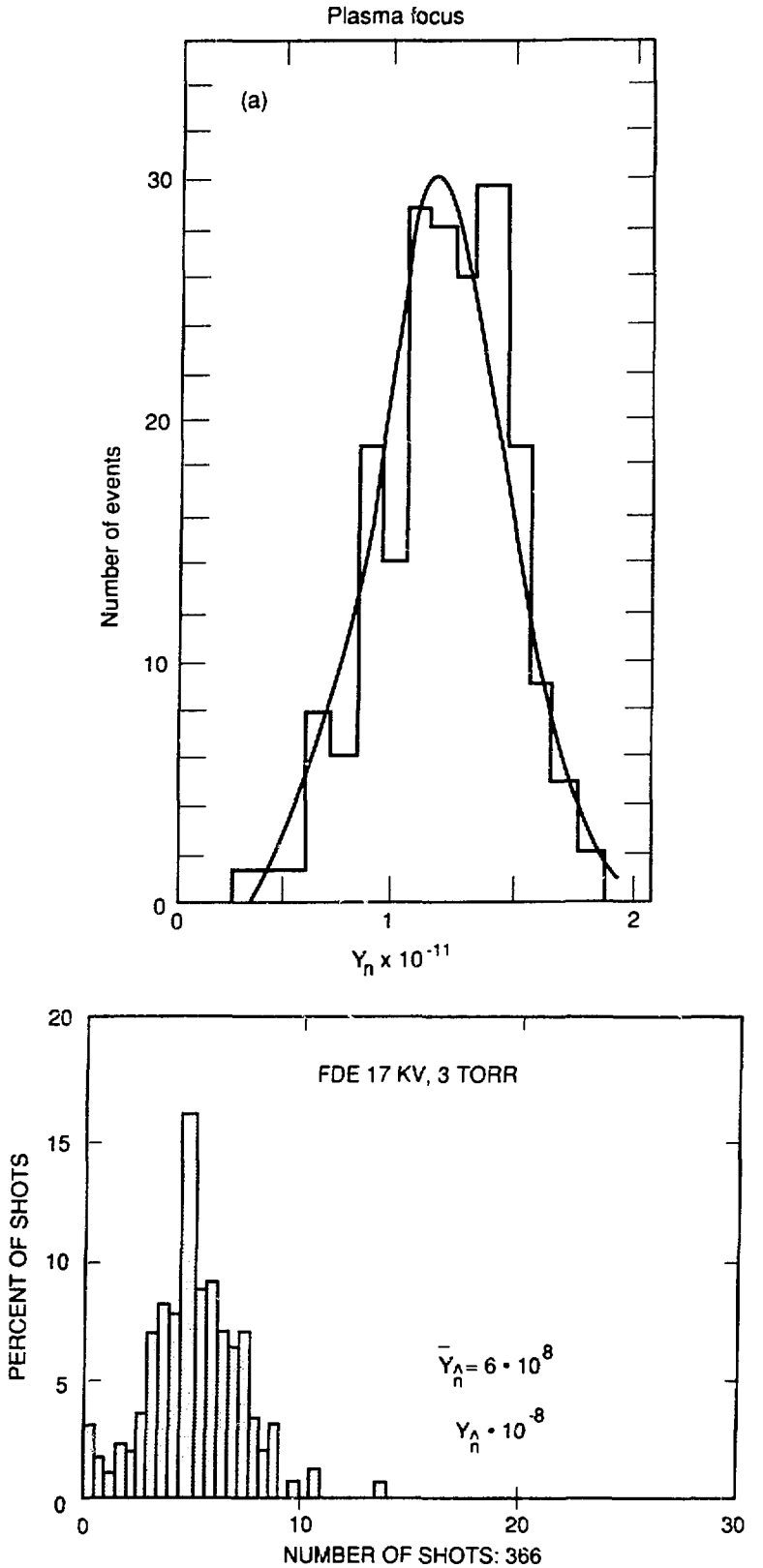

Fig. 8 (a) Number of shots as a function of the observed neutron yield Y_n for the Frascati PF machine without FDE (conventional PF type) 250 kJ ≤ $W_{0,F}$ ≤ 560 kJ, for different values of the D_2 filling pressure P (3 Torr ≦ P≦ 8 Torr); see Ref. 9. (b) Percentage of shots (as a fraction of the total number of shots under the same conditions) from two identical APFs (Stevens Tech and University of Ferrara, Italy; $W_{0,H}$ = 6 kJ); $\bar{Y}_n$ is the mean value of Y_n from all shots; see Ref. 2.

(i) operation at very high voltage[10] (up to 300 kV as in the Düsseldorf experiments) or (ii) use of the FDE of an Advanced Plasma Focus system. The latter method is much less expensive than the high-voltage operation and at least equally effective[2,10].

A neutron radiography demonstration using a single-step contrast system has been successfully carried out since 1975 by using a PF ($Y_n = 10^9$ - 10^{10} of D-D (~2.5 MeV) neutrons) with W_0 = 30 kJ[11]. The experimental set up and the results are shown in Fig. 9. A comparison of different neutron sources and the expected results from an APF for neutron radiography is presented in Appendix I and in Fig. 10.

III. Slow and Fast Neutron Radiography with Advanced Plasma Focus Systems

A spherical (> 3 π sector) moderator with collimator can be fitted on the cylindrical wall of the APF discharge chamber, which has a diameter slightly greater (e.g., by ~2 cm) than the diameter of the APF outer electrode (cathode; the cathode can also become the wall of the discharge chamber by extending the cathode length by a few centimeters and by closing its front end in a configuration similar to the Filippov-PF electrode geometry)[1]. The APF cathode has the following typical diameters: ~6 cm if W_0 ~1 to 2 kJ (Y_n ~10^{10} 14-MeV neutrons from D-T reactions, or Y_n ~10^8 2.5-MeV neutrons from D-D reactions); ~10 cm for W_0 ~5 to 8 kJ (Y_n ~2 x 10^{11} or ~2 x 10^9); and ~20 cm for W_0 ~180 kJ (Y_n ~10^{14} or Y_n ~10^{12}). An APF with moderator can be used as a convenient source of low-energy (thermal[12], epithermal[13], etc.) neutrons of high intensity and with a mobility predominantly dictated by the moderator weight. For a chosen APF, the space resolution is defined as in other systems by the moderator structure and the collimator L/D factor. The time resolution is reduced to the neutron-pulse thermalization time (ms). The neutron loss at the moderator surface requires a relatively high value of W_0 (e.g., ~200 kJ), but with a corresponding weight of the capacitor bank still substantially smaller than that of the moderator. The structure of a layered-material moderator (metallic internal layer and, e.g., polyethylene or solid-methane outer layer[14]) can be designed with the help of a powerful Monte Carlo numerical code, e.g., the advanced version of 3 DAMV-VINIA with a continuous representation of energy and space variables[15]. A careful design can minimize the moderator linear dimensions (i.e., weight and neutron loss) for chosen constraints on neutron beam energy and angular spread. Tailoring the moderator design to a specific radiographic application may increase the available intensity of the slow-neutron beam by orders of magnitude without increasing W_0. This provides

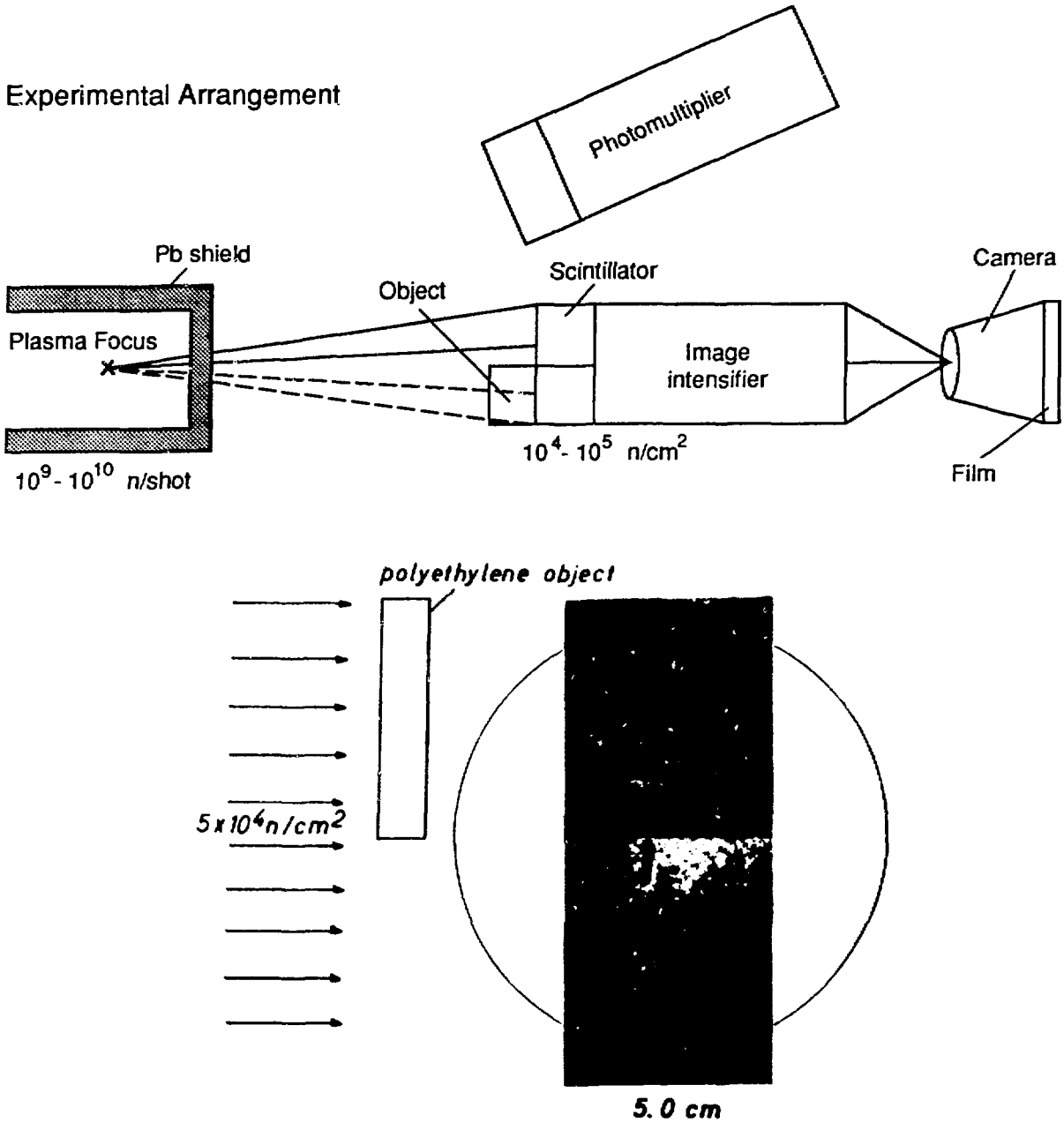

Fig. 9 Upper side: Experimental arrangement of the first neutron-radiography test with 2.5 MeV neutrons (from D-D reactions, $Y_n = 10^{10}$) from a conventional PF with $W_0 = 30$ kJ at Stuttgart University (see Ref. 11).
Lower side: Film contrast behind polyethylene plate 5.0-cm-thick. The circle is the circumference of the scintillator (a 25-mm-thick plate of NE-102), which was optically divided. Distance of the object to the source is 1.2 m.

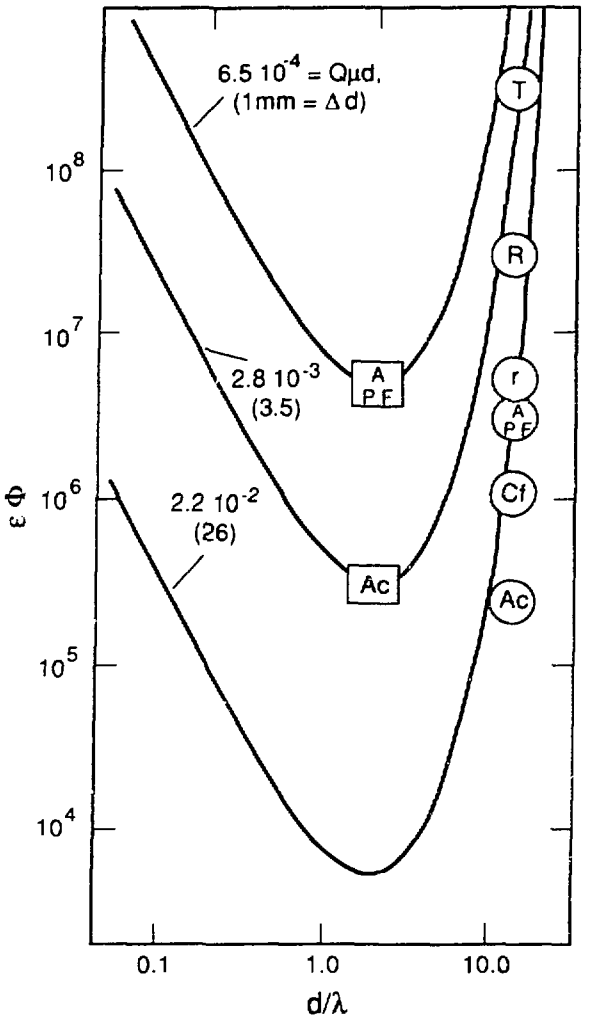

Fig. 10. The effective illumination, $\varepsilon\,\phi$, of the surface of the recording system, required for a constant resolution of a void characterized by $\mu \times \rho \times \rho$ (cm^2), is plotted as a function of the object thickness d/λ (neutron mean-free path λ as a unit.). Each solid curve corresponds to a specific value with $\rho\mu$ = constant. The corresponding numerical value $\rho\mu d$ is used to label each curve; a constant factor $d_1 \equiv 12$ cm—the thickness of a slab of Fe about twice the mean-free path of a 14-MeV neutron in Fe—is entered for having a dimensionless quantity; the depth Δd of the void in mm, if $\rho = 1$ mm, is also indicated in brackets. For an assessment of the performance of different neutron sources (APF, R, AC, Cf, T), we consider a range of d/λ (horizontal axis), which fits a 9 to 15 cm thick object (λ corresponds to a medium value of A) and an exposure time $\cong$ 1 min. (or, alternatively, the exposure of one APF pulse). Squares and circles correspond to fast and quasi-thermal neutrons, respectively. APF is the advanced plasma focus (10^{14} n/shot); AC is the accelerator with an expected upper limit of neutron production $\cong 10^{11}$ n/s); R is a 5-MW reactor[23]; r is a reactor especially designed for neutron radiography[23]; Cf is the 5 mg ^{252}Cf subcritical assembly[23]; T is the TRIGA reactor with a 9-ms pulse[20].

additional flexibility to the APF source for which a modular organization of the powering capacitor bank, at a relatively low voltage (20 to 60 kV), can be exploited for operating at different values of W_0 without elaborate modifications of the system.

The major advantages of an APF—mobility, extreme time resolution (~50 to 100 ns), excellent space resolution ($L/D \gtrsim 300$ to 600)—as compared to other accelerator sources from D-T reactions (e.g., the Kaman Instrumentation Corporation's A-711 model[12] or from photoneutron reactions[16]) can be fully exploited in radiography with fast neutrons. The resolution is particularly increased by the absence of a moderator because of the extreme localization of the source core.

Time-integrated radiographic images with 14-MeV neutrons have been reported in the literature[17,18,19]. Images of good quality have been obtained so far with the use of collimators, which were required in those tests because of the spatial extension of the neutron source. In our estimate, an APF without a collimator can provide radiographic images of better quality—at least of the same quality as the x-ray radiography images that have been obtained with a PF as a point x-ray source. The neutron source has the same extension of, and is superposed to, the x-ray source in time and space. Full advantage is taken of the unique characteristic of the source if the source is matched with a fast neutron detector. In this case, the time resolution for real-time radiography is established by the response speed of the imaging system, i.e., orders of magnitude higher than the time resolution reported in the literature[20].

The feasibility of real-time radiography with APF fast neutrons ultimately depends on and is reduced to the problem of developing fast-neutron detectors similar (but with substantial innovations) to the microchannel plate detectors of reported pioneering work that used neutrons of relatively low energy[21]. Further complexity is introduced in the problem of image formation with MeV neutrons, from the x- and γ- ray contributions to the background, which, in this case, cannot be eliminated by using transfer methods[17,22].

Appendix I

A worldwide effort is presently under way for developing a high-intensity, mobile neutron source for neutron radiography (real-time radiography) of material surfaces or of bulk

objects. This source needs to fit field-use requirements[12,13,14,16-22], which include minimization of radiation hazards, construction and operation costs, transportation difficulties, and increased reliability.

Motivations for the use of neutron radiography are provided by increased requirements on materials and by the fact that neutron radiography detects and/or images corrosion, trapped moisture, adhesive bonding flaws, voids, cracks, porosity, fuel-leakage paths, O-ring conditions, and other hidden flaws. The advantage of using neutrons over x-rays in these tests rests on the dependence of the radiation attenuation on the atomic species that constitutes the object: the x-ray attenuation is rapidly increasing with the atomic number Z of the elements, while the major factor in determining the attenuation for neutrons is the density of the nuclei with a relatively weak dependence of the nuclear mass number A. Neutrons penetrate deeper than x-rays; in particular, most metals that readily absorb x-rays are relatively transparent to neutrons.

The main parameter that defines the final success of neutron imaging is the spatial resolution on the recorded image that the system can provide. The spatial resolution is characterized by two factors, ρ and μ. A commonly used factor, ρ, defines the transversal resolution of the image and is defined by the width δ of the source and by the ratio of the distance/object recording system, d_o, to the distance, $\bar{L}$, object-source, $\rho = \delta\, d_o/\bar{L}$. The second factor, $\mu = \Delta d/d$ (where Δd is the length of the void or defect in the direction of the incoming neutron beam; d is the thickness of the object in which the void is embedded), is representative of the statistical fluctuations of neutron-induced luminosity in the image-recording system. The criterion for determining the possibility of detecting a void, defect, etc., inside the object is

$|I-I'| > \beta\sqrt{I}$, where $\beta \geq 1$ is a factor chosen for expressing the quality of the considered resolution. I and I' are defined as follows:

- $I = \pi(\rho_o^2/4)\, \phi \exp(-d/\lambda)$ is the number of neutrons impinging on the recorder surface on a circular area of diameter ρ_o and with a trajectory not crossing the void, defect, etc., to be detected by the radiography.

- $I' = \pi(\rho_o^2/4)\, \phi \exp[(d - \Delta d)/\lambda - \Delta d/\lambda']$ is the number of neutrons impinging on the recorder surface but passing through the void, defect, etc., of diameter not smaller than ρ and thickness, Δd,

where

$$\phi = Y_n/4\pi\,(\bar{L} + d_o)^2 \equiv Y_n/4\pi\bar{L}^2$$

is the illumination of the object .

- Y_n is the total yield of the neutron source: for fast neutrons, Y_n is the actual source yield; for slow neutrons, Y_n is the quantity of neutrons emitted by the element of the external surface of the neutron moderator subtended by the neutron collimator aperture (at the collimator entrance).

- d is the longitudinal dimension of the object ($d << d_o, \bar{L}$).

- $\lambda = \Sigma\, n_i\, \sigma_i$ is the neutron mean-free path, σ_i the total cross section, and n_i is the density of nuclei of the *ith* type along the neutron trajectory in the object.

The relation connecting the illumination of the object, the recorder efficiency ε, and the object thickness (as expressed in terms of neutron mean-free path units d/λ) for a particular (relative) longitudinal resolution, $\mu = \Delta d/d$, and transversal resolution, ρ, is expressed as:

$$\varepsilon\phi = \frac{4}{\pi}\left(\frac{\beta}{\rho\mu}\right)^2\left(\frac{\lambda'}{\lambda' - \lambda}\right)^2\left(d/\lambda\right)^{-2}\exp\left(d/\lambda\right).$$

If a void, cavity, defect, etc., is considered, then

$$\varepsilon\phi = \frac{4}{\pi}\left(\frac{\beta}{\rho\mu}\right)^2\left(\frac{d}{\lambda}\right)^{-2}\exp\left(d/\lambda\right).$$

Fig. 10 gives the dependence of $\varepsilon\phi$ on d/λ for a specific dimension cavity and, additionally, for the case $\beta = 1$, which corresponds to a convenient upper limit for μ and ρ. Usually for high-quality radiography, a value $\beta = 3$ is a requirement.

The above discussion agrees with well-known experimental facts, i e., that success and improvements of neutron radiography are based on the high fluence of neutrons on the

recorder surface because of the high efficiency of the presently used neutron recording systems.

High quality radiography is possible with some 10^9 recorded neutrons/cm^2 on the average. On the other hand, as few as 10^4 recorded neutrons/cm^2 are sufficient for producing a recognizable image of a variety of objects. Consistently, in the case of an image-recording element with a neutron-recording efficiency of 10% for quasi-thermal neutrons (1% for fast neutrons), and if 10% of the neutrons pass through the object, we must have a minimum of 10^6 n/cm^2 (10^7 n/cm^2 for fast neutrons) falling on the object plane during the time of the radiography. Problems of neutron illumination do not exist when a high-power fission reactor (e.g., a 3000-MW peak-power TRIGA reactor) is used where the peak neutron flux incident on the object is ~4.10^{11} neutrons/cm^2/s with a pulse (FWHM) of 9 ms[20]. On the other hand, when a mobile accelerator is used as a neutron source and generates typically 10^{10} fast neutrons/s, only 10^4 quasi-thermal neutrons/cm^2/s of continuous beam are available and can be used for the radiography of thin objects with a 10-min. exposure time[12]. This seems to be, and presently is, the upper limit of an accelerator performance.

The above observations indicate that the development of neutron radiography beyond the present limits requires a new concept of a mobile compact source if the requirement must be met of having neutron sources more intense by at least two orders of magnitude than the intensity provided by an accelerator. An APF can provide a sufficiently high neutron flux in 100-ns pulses.

References

1. J. W. Mather: Methods of Experimental Physics, 9, Part B, (R. H. Lowberg and H. R. Griem, Eds.), New York, Academic Pr. 1971, p. 187

2. V. Nardi, et al: Proc. 13th Eur. Conf. Controlled Fusion and Plasma Physics (Schliersee, FRG), 1986, Vol. 10-C-1, p. 368 and IEEE Trans. Plasma Science, Vol. 16, 369 (1988) and 16, 374 (1988). V. Nardi, U.S. Patent Application 07-037-753, Apr. 13, 1987

3. O. Zucker, W. H. Bostick, R. Gullickson, J. Long, J. Luce, H. Sahlin: "The Design of a Repetitively Pulsed Megajoule Dense-Plasma Focus", Lawrence Livermore Lab. Report UCRL-51872 (Dis. Cat. UC-38), Aug. 1, 1975. V. Nardi: Proc. Int. Conf. on Radiation Test Facilities for the CTR Surface and Material Program, Argonne, July 15-18, 1975; ANL Report ANL/CTR 75-4, (Persiani edit.), p. 527

   A. Bernard, et al: Nuclear Instr. & Meth., 145, 191 (1977)

4. J. Salge, et al: Nuclear Fusion, 18, 972 (1978) and Energy Storage, Compression and Switching, 2, 75 (1983), Plenum, NY

   H. Conrads, J. Salge, Energy Storage, Comp. & Switch, 2, 87 (1984), NY

   P. Cloth, H. Conrads, B. Giesen, F. Schongen: Proceedings Ninth SOFT Conference (1976), p. 597-604

   J. Kucinski, A. Jerzykiewicz: Proc. 4th Int. Workshop on Plasma Focus & Z-Pinch Research (Warsaw, Sept. 9-11, 1985), p. 47, Publish. Inst. of Plasma Physics & Laser Microfusion, Warsaw, Poland

5. W. H. Bostick, V. Nardi, W. Prior: Nuclear Fusion, Suppl. 3, 497 (1977)

6. W. H. Bostick, V. Nardi, W. Prior: J. Plasma Physics, 8, 7 (1972)

7. W. H. Bostick, et al: Energy Storage, Comp. & Switch., (Plenum Pub. Co., New York, 1984) 2, p. 267

8. G. Decker, R. Wienecke: Physica, 82C, 155 (1976)

9. J. S. Brzosko, J. Klobukowska, B. V. Robouch: "Time Sequences in the Neutron γ- and X-ray Emission in the Frascati Plasma Focus", ENEA Report RT/FUS/84/6, Frascati, Italy, (June 1984)

10. G. Decker, et al: Proc. 11th European Conf. Controlled Fusion and Plasma Physics, Aachen, FRG, Sept. 5-9, 1983 (S. Methfessel ed., EPS), p. 501

11. H. Rapp, E. Rouchle, D. Ruffner: Materials Evaluation, 33, 269 (Nov. 1975)

12. W. E. Dance, S. F. Carollo, H. M. Bumgardner: "Mobile Accelerator Neutron Radiography", LTV Aerospace and Defense Company -Vought Missiles andAdvanced Programs Division (Dallas, Texas 75265-0003), Report AMMRC TR 84-39, Oct. 1984

13. P. H. Fowler, A. D. Taylor: "Temperature Imaging Using Epithermal Neutrons", Rutherford-Appleton Lab. (Chilton, UK), Report RAL-87-056 (Aug. 1977) and these proceedings

14. J. M. Carpenter, et al.: Proceed. 8th Meeting Intl. Collaboration on Advanced Neutron Sources (ICANS-VIII) Rutherford Appleton Lab, July 8-12, 1985, Report RAL-85-110, 1, p. 311, (Nov. 1985)

15. J. S. Brzosko, B. V. Robouch, and L. Ingrosso: IEEE Trans. of Plasma Sciences, PS-15, 16 (1987) and literature quoted therein

16. R. G. Johnson, R. A. Schrack: "Nondestructive Evaluation of M732 Proximity Fuses", Natl. Bureau of Standards Report NBSIR 85-3259, Nov. 1985 (Gaithersburg, MD)

17. H. Berger: Materials Evaluations, 27, 245 (Dec. 1969)

18. A. E. Richardson: Materials Evaluation, 35, 52, (1977)

19. E. Bagge, et al: Nucl. Instr. and Meth., 147, 109, (1977)

20. R. H. Bossi, A. H. Robinson, J. P. Barton: "High-Frame Rate Neutron Radiography of Dynamic Events", Lawrence Livermore Nat. Lab. Report UCRL-86954 (DE82-004389), and Proceed. World Conf. on Neutron Radiography, San Diego, CA, Dec. 7-10, 1981

21. R. A. Schrack: "A Microchannel Plate Neutron Detector: International Advances in Nondestructive Testing", 2, p 219-249, (1985) Gordon and Breach.(UK)

22. R. H. Bossi, J. L. Cason, C. N. Jackson, Jr: Materials Evaluation, 30, 103, (May 1972)

23. D. E. Wood, Tans Am. Nucl. Soc, 10, 443, (1967)

H. Berger, "Neutron Radiography", Elsevier Pub. Co., New York, 1965

J. P. Barton, P. von Der Hardt: "Neutron Radiography", Boston, MA, D. Reidel Publ. Co, 1983

M. R. Hawkesworth, Atomic Energy Rev. 152, 169 (1977)